Journal of Solid State Chemistry 181 (2008) 2690–2696

Contents lists available at ScienceDirect

Journal of Solid State Chemistry

journal homepage: www.elsevier.com/locate/jssc

# Synthesis, structure and physical properties of the new Zintl phases $Eu_{11}Zn_6Sb_{12}$ and $Eu_{11}Cd_6Sb_{12}$

Bayrammurad Saparov [a], Svilen Bobev [a,*], Arif Ozbay [b], Edmund R. Nowak [b]

[a] Department of Chemistry and Biochemistry, University of Delaware, Romm 304A, Drake Hall, Newark, DE 19716, USA
[b] Department of Physics and Astronomy, University of Delaware, Newark, DE 19716, USA

ARTICLE INFO

*Article history:*
Received 7 April 2008
Received in revised form
17 June 2008
Accepted 22 June 2008
Available online 1 July 2008

*Keywords:*
Zintl phases
Crystal structure
X-ray diffraction
$Eu_{11}Zn_6Sb_{12}$
$Eu_{11}Cd_6Sb_{12}$

ABSTRACT

Reported are the syntheses, crystal structure determinations from single-crystal X-ray diffraction, and magnetic properties of two new ternary compounds, $Eu_{11}Cd_6Sb_{12}$ and $Eu_{11}Zn_6Sb_{12}$. Both crystallize with the complex $Sr_{11}Cd_6Sb_{12}$ structure type—monoclinic, space group $C2/m$ (no. 12), $Z=2$, with unit cell parameters $a=31.979(4)$ Å, $b=4.5981(5)$ Å, $c=12.3499(14)$ Å, $\beta=109.675(1)^\circ$ for $Eu_{11}Zn_6Sb_{12}$, and $a=32.507(2)$ Å, $b=4.7294(3)$ Å, $c=12.4158(8)$ Å, $\beta=109.972(1)^\circ$ for $Eu_{11}Cd_6Sb_{12}$. Their crystal structures are best described as made up of polyanionic $^1_\infty[Zn_6Sb_{12}]^{22-}$ and $^1_\infty[Cd_6Sb_{12}]^{22-}$ ribbons of corner-shared $ZnSb_4$ and $CdSb_4$ tetrahedra and $Eu^{2+}$ cations. A notable characteristic of these structures is the presence of Sb–Sb interactions, which exist between two tetrahedra from adjacent layers, giving rise to unique channels. Detailed structure analyses shows that similar bonding arrangements are seen in much simpler structure types, such as $Ca_3AlAs_3$ and $Ca_5Ga_2As_6$ and the structure can be rationalized as their intergrowth. Temperature-dependent magnetization measurements indicate that $Eu_{11}Cd_6Sb_{12}$ orders anti-ferromagnetically below 7.5 K, while $Eu_{11}Zn_6Sb_{12}$ does not order down to 5 K. Resistivity measurements confirm that $Eu_{11}Cd_6Sb_{12}$ is poorly metallic, as expected for a Zintl phase.



## 1. Introduction

Zintl phases attract much attention from a fundamental standpoint because of the appeal of their diverse crystal and electronic structures [1–3]. Recently, reports on unusual magnetic, electronic and thermoelectric properties within the realm of some ternary Zintl phases [4–9] have generated renewed interest in these materials from a practical position, and have opened new research opportunities for solid-state chemists.

In the past 2–3 decades, the traditional Zintl boundaries have been extended to include some of the lanthanides and the transition metals [3]. Many such compounds have already been synthesized and structurally characterized [3–11]; however, quite surprisingly, much phase space still remains unexplored. A brief survey of the literature from the last 5–8 years reveals a wealth of new bonding patterns and properties within the ternary manganese pnictides alone—$Sr_{21}Mn_4Sb_{18}$ [12], $EuMn_2P_2$ [13], $Sr_2MnSb_2$ [14], $CaMn_2Sb_2$ [15], $Eu_{10}Mn_6Sb_{13}$ [16], $Ca_{21}Mn_4Bi_{18}$ [17], among others. These recent findings, together with the fact that there are great similarities between the crystal chemistry of Mn- and many of the Zn- and Cd-compounds, the structures of which are often based on isolated or condensed tetrahedra, inspired us to begin systematic studies on the chemistry and properties of other members of this potentially very large family.

We have already reported on several new compounds in the *A*–Zn–*Pn* and *A*–Cd–*Pn* systems (*A* = divalent alkaline- or rare-earth metals; *Pn* = pnicogen). Some specific examples include: $Ba_{11}Cd_8Bi_{14}$ [18], $Yb_2CdSb_2$ and $Ca_2CdSb_2$ [19], $Eu_{10}Cd_6Bi_{12}$ [20], $Sr_{21}Cd_4Sb_{18}$ and $Ba_{21}Cd_4Sb_{18}$ [21], $Ba_{11}Cd_6Sb_{12}$ [22]. Herein, we provide new results from these ongoing efforts by reporting the syntheses and the structural characterization of the first Eu-compounds with the *C*-centered monoclinic $Sr_{11}Cd_6Sb_{12}$ type (Pearson's symbol *mC*58) [23], $Eu_{11}Zn_6Sb_{12}$ and $Eu_{11}Cd_6Sb_{12}$. This structure is based on antimony tetrahedra centered by Zn or Cd atoms, which share corners to form a unique polyanionic ribbons. Since the subtleties of this bonding arrangement and its electronic requirements have been discussed at length elsewhere [22,23], the focus of this paper is on the "structural genealogy" of the structure and its similarities with the structures of other well-known ternary Zintl phases. Aside from this comparative analysis, we also discuss the complicated phase relationships in the corresponding phase diagrams, as well as the temperature dependence of the magnetization of both $Eu_{11}Zn_6Sb_{12}$ and $Eu_{11}Cd_6Sb_{12}$. Resistivity data taken on a single-crystal of $Eu_{11}Cd_6Sb_{12}$ are also presented.

* Corresponding author. Fax: +1 302 831 6335.
*E-mail address:* bobev@udel.edu (S. Bobev).

0022-4596/$ - see front matter © 2008 Elsevier Inc. All rights reserved.
doi:10.1016/j.jssc.2008.06.054

## 2. Experimental

### 2.1. Synthesis

All manipulations were carried out in an argon-filled glove box or under vacuum. The metals were purchased from Alfa or Aldrich and were used as received: Eu (ingots, 99.9%), Sb (shot, 99.99%), Zn (shot, 99.999%), Cd (shot, 99.999%), Ca (granules, 99.9%), Pb (granules, 99.999%). Pb-flux reactions in alumina crucibles [24] and on-stoichiometry reactions in welded niobium tubes were employed for the syntheses. To prevent oxidation, heating of the reaction mixtures was done in evacuated fused silica ampoules. Details on the procedures can be found elsewhere [24].

$Eu_{11}Cd_6Sb_{12}$ was initially identified as a product of a reaction of Eu, Cd and Sb in Pb flux (ratio of Eu:Cd:Sb:Pb = 10:6:13:50), loaded in an attempt to synthesize the Cd analog of $Eu_{10}Mn_6Sb_{13}$ [16]. The mixture was heated to 950 °C at a rate of 10 °C/h; allowed to stay at this temperature for 24 h, and then cooled to 550 °C at a rate of 5 °C/h. After a 96 h annealing at 550 °C, the excess of molten lead was removed by a centrifugation. The fused silica ampoule was brought back in the glove box and opened. The reaction outcome consisted of black, needle-like crystals, later identified as $Eu_{11}Cd_6Sb_{12}$. The estimated yield was greater than 50%.

After the $Eu_{11}Cd_6Sb_{12}$ structure was established by X-ray crystallography, the reaction conditions were optimized and the synthesis was repeated with the ratio of Eu:Cd:Sb = 11:6:12 (≈2:1:2). Pb-flux reactions (20-fold excess) proved to be the optimal method for the synthesis of sizeable single crystals of $Eu_{11}Cd_6Sb_{12}$ and without any side products. Crystals of the isostructural $Eu_{11}Zn_6Sb_{12}$ were successfully grown from a Pb flux as well. The latter reactions also produced another, presumably hexagonal phase, the structure of which is not known yet. Both $Eu_{11}Cd_6Sb_{12}$ and $Eu_{11}Zn_6Sb_{12}$ appear to be sensitive to air.

Attempts to synthesize analogous compounds in the systems *A*–*M*–*Pn*, where *A* = Ca, Sr, Ba, Eu, Yb; *M* = Cd, Zn; and *Pn* = Sb, Bi were also undertaken. Different fluxes (In, Cd, Pb and Sn) were tried, but only $Ba_{11}Cd_6Sb_{12}$ [22] and $Sr_{11}Cd_6Sb_{12}$ [23] could be synthesized. In all other instances, the products of the reactions were among the following known compounds: $Ba_{11}Cd_8Bi_{14}$ [18], $Yb_2CdSb_2$ and $Ca_2CdSb_2$ [19], $Eu_{10}Cd_6Bi_{12}$ [20], $Ba_{21}Cd_4Sb_{18}$ and $A_{21}Cd_4Bi_{18}$ [21], $Ba_2Cd_3Bi_4$ [25], $A_9M_{4+x}Pn_9$ [26], $AM_2Pn_2$ [27], $Ca_{14}CdSb_{11}$ [28], $CaCd_6$, $ACd_{11}$ and $A_{11}Pn_{10}$ binaries [29]. The new phase $Sr_{21}Cd_4Sb_{18}$, isostructural with $Sr_{21}Cd_4Bi_{18}$ [21], was also synthesized [30].

Two general observations from the above-mentioned elaborate syntheses must be pointed out: (1) Despite all the attempts, employing both flux and stoichiometric reactions, no Bi analogs could be synthesized; and (2) Regardless of the heat treatment, stoichiometric reactions in sealed tubes could not produce neither $Eu_{11}Cd_6Sb_{12}$ nor $Eu_{11}Zn_6Sb_{12}$ in large yields. Similar findings are reported for the Sr- and Ba-analogs, synthesized in Sn and Pb flux, respectively [22,23]. Since there are no indications of Sn or Pb solubility in the structure, all of the above likely indicates that $Sr_{11}Cd_6Sb_{12}$, $Ba_{11}Cd_6Sb_{12}$, $Eu_{11}Cd_6Sb_{12}$ and $Eu_{11}Zn_6Sb_{12}$ are metastable phases, which can be "trapped" using the flux method [24]. These traits are discussed in a broader context later on.

### 2.2. Crystallographic studies

X-ray powder diffraction patterns were taken on a Rigaku MiniFlex powder diffractometer, using nickel-filtered Cu *K*α radiation. The instrument was enclosed and operated inside a nitrogen-filled glove box. This was done so that data can be acquired for air- and/or moisture-sensitive samples. Due to the complexity of the structure and the limited instrument resolution, satisfactory refinements of the unit cell parameters or the structure could not be achieved. The collected powder diffraction patterns were only used for phase identification, which was done using the JADE 6.5 package [31].

Single-crystal X-ray diffraction data were acquired using a Bruker SMART CCD-based diffractometer and monochromated Mo *K*α radiation. To circumvent the problem with the air-sensitivity of the samples, single-crystal of $Eu_{11}Cd_6Sb_{12}$ and $Eu_{11}Zn_6Sb_{12}$ were selected in the glove box. The crystals were mounted on glass fibers using Paratone N oil and quickly transferred onto the goniometer, equipped with a low-temperature device (liquid nitrogen evaporator). A full sphere of reciprocal space data were collected in four-batch runs with scans in different $\omega$ and $\phi$ angles using the SMART [32] software. SAINTplus software package was used for the integration and the cell refinement [33]; semi-empirical absorption correction based on equivalents was applied with SADABS [34]. Since the structures were of a known type, the atomic positions were assigned according to the established model [22]. Structure refinements were carried out with SHELXL [35] using the full matrix least-squares method on $F^2$. All sites were refined with anisotropic displacement parameters. Important data collection and structure refinement information is provided in Table 1. Positional and equivalent isotopic displacement parameters, and relevant interatomic distances are listed in Tables 2–4, respectively. Further details of the crystal structure investigations can be obtained from Fachinformationszentrum Karlsruhe, 76344 Eggenstein-Leopoldshafen, Germany; (fax: (+49) 7247 808 666; or e-mail: crysdata@fiz.karlsruhe.de) on quoting the depository numbers: CSD 419343 ($Eu_{11}Zn_6Sb_{12}$) and CSD 419344 ($Eu_{11}Cd_6Sb_{12}$).

### 2.3. Magnetic susceptibility measurements

Field-cooled magnetization measurements were performed in a Quantum Design MPMS2 SQUID from 5 to 300 K in a magnetic field (*H*) of 500 Oe. Single crystals of $Eu_{11}Cd_6Sb_{12}$ and $Eu_{11}Zn_6Sb_{12}$ were selected in the glove box (under a microscope) and secured in a custom-designed sample holder for air-sensitive materials [18]. Raw data were corrected for diamagnetic contribution from the holder and converted to molar magnetic susceptibility ($\chi_m = M/H$) in emu/mol-Eu units.

**Table 1**
Selected single-crystal data collection and refinement parameters for $Eu_{11}Cd_6Sb_{12}$ and $Eu_{11}Zn_6Sb_{12}$

| | | |
|---|---|---|
| Formula | $Eu_{11}Cd_6Sb_{12}$ | $Eu_{11}Zn_6Sb_{12}$ |
| Formula weight | 3806.96 | 3524.78 |
| Radiation | Mo *K*α, 0.71073 Å | |
| Crystal system | Monoclinic | |
| Space group | *C*2/*m* (no. 12) | |
| Temperature | 120(2) K | |
| Unit cell parameters | *a* = 32.507(2) Å | *a* = 31.979(4) Å |
| | *b* = 4.7294(3) Å | b = 4.5981(5) Å |
| | *c* = 12.4158(8) Å | c = 12.3499(14) Å |
| | *β* = 109.972(1) | *β* = 109.675(1) |
| Volume, *Z* | 1794.0(2) Å$^3$, 2 | 1709.9(3) Å$^3$, 2 |
| Density ($\rho_{calc}$) (g/cm$^3$) | 7.048 | 6.846 |
| Absorption coefficient ($\mu$) (mm$^{-1}$) | 31.207 | 33.218 |
| Transmission factors, min/max | 0.0796/0.534 | 0.2144/0.3980 |
| Crystal size (mm$^3$) | 0.16 × 0.08 × 0.02 | 0.07 × 0.04 × 0.03 |
| Reflections collected | 9631 | 9144 |
| Independent reflections | 2055 | 1972 |
| Final $R_1$ ($I > 2\sigma_{(I)}$)[a] | 0.0172 | 0.0264 |
| Final w$R_2$ ($I > 2\sigma_{(I)}$)[a] | 0.0359 | 0.0563 |
| Largest peak/hole (e$^-$/Å$^3$) | 1.0/−1.31 | 1.67/−2.31 |

[a] $R_1 = \sum ||F_o| - |F_c|| / \sum |F_o|$; $wR_2 = [\sum[w(F_o^2 - F_c^2)^2] / \sum[w(F_o^2)]]^{1/2}$, where $w = 1/[\sigma^2 F_o^2 + (0.0078P)^2 + 9.6977P]$ for $Eu_{11}Cd_6Sb_{12}$ and $w = 1/[\sigma^2 F_o^2 + (0.0137P)^2 + 74.6291P]$ for $Eu_{11}Zn_6Sb_{12}$. $P = (F_o^2 + 2F_c^2)/3$.

**Table 2**
Atomic coordinates and equivalent isotropic displacement parameters ($U_{eq}$)[a] for $Eu_{11}Cd_6Sb_{12}$

| Atom | Wyckoff site | $x$ | $y$ | $z$ | $U_{eq}$ (Å$^2$) |
|---|---|---|---|---|---|
| Eu1 | 4*i* | 0.01909(1) | 0 | 0.68073(3) | 0.0087(1) |
| Eu2 | 4*i* | 0.11391(1) | 0 | 0.50687(3) | 0.0080(1) |
| Eu3 | 4*i* | 0.12575(1) | 0 | 0.01556(3) | 0.0087(1) |
| Eu4 | 4*i* | 0.19975(1) | 0 | 0.34234(3) | 0.0088(1) |
| Eu5 | 4*i* | 0.27711(1) | 0 | 0.13199(4) | 0.0096(1) |
| Eu6 | 2*a* | 0 | 0 | 0 | 0.0081(1) |
| Cd1 | 4*i* | 0.21991(2) | 0 | 0.66593(5) | 0.0093(1) |
| Cd2 | 4*i* | 0.39854(2) | 0 | 0.25347(5) | 0.0091(1) |
| Cd3 | 4*i* | 0.54753(2) | 0 | 0.24742(5) | 0.0109(1) |
| Sb1 | 4*i* | 0.08981(2) | 0 | 0.23314(4) | 0.0078(1) |
| Sb2 | 4*i* | 0.15129(2) | 0 | 0.78539(4) | 0.0076(1) |
| Sb3 | 4*i* | 0.30928(2) | 0 | 0.47150(5) | 0.0079(1) |
| Sb4 | 4*i* | 0.45335(2) | 0 | 0.11501(4) | 0.0075(1) |
| Sb5 | 4*i* | 0.45662(2) | 0 | 0.49900(4) | 0.0076(1) |
| Sb6 | 4*i* | 0.70360(2) | 0 | 0.13411(4) | 0.0076(1) |

[a] $U_{eq}$ is defined as one-third of the trace of the orthogonalized $U_{ij}$ tensor.

**Table 3**
Atomic coordinates and equivalent isotropic displacement parameters ($U_{eq}$)[a] for $Eu_{11}Zn_6Sb_{12}$

| Atom | Wyckoff site | $x$ | $y$ | $z$ | $U_{eq}$ (Å$^2$) |
|---|---|---|---|---|---|
| Eu1 | 4*i* | 0.01833(2) | 0 | 0.67866(6) | 0.0082(2) |
| Eu2 | 4*i* | 0.11448(2) | 0 | 0.50863(6) | 0.0078(2) |
| Eu3 | 4*i* | 0.12608(2) | 0 | 0.02037(6) | 0.0085(2) |
| Eu4 | 4*i* | 0.19953(2) | 0 | 0.34530(6) | 0.0086(2) |
| Eu5 | 4*i* | 0.28054(2) | 0 | 0.13556(6) | 0.0094(2) |
| Eu6 | 2*a* | 0 | 0 | 0 | 0.0086(2) |
| Zn1 | 4*i* | 0.21737(5) | 0 | 0.6728(1) | 0.0098(3) |
| Zn2 | 4*i* | 0.40098(5) | 0 | 0.2552(1) | 0.0093(3) |
| Zn3 | 4*i* | 0.54579(5) | 0 | 0.2429(1) | 0.0116(3) |
| Sb1 | 4*i* | 0.08645(3) | 0 | 0.23549(7) | 0.0076(2) |
| Sb2 | 4*i* | 0.14605(3) | 0 | 0.78196(7) | 0.0076(2) |
| Sb3 | 4*i* | 0.30760(3) | 0 | 0.45699(7) | 0.0078(2) |
| Sb4 | 4*i* | 0.45361(3) | 0 | 0.12030(7) | 0.0072(2) |
| Sb5 | 4*i* | 0.45574(3) | 0 | 0.49539(7) | 0.0074(2) |
| Sb6 | 4*i* | 0.70640(3) | 0 | 0.14209(7) | 0.0080(2) |

[a] $U_{eq}$ is defined as one-third of the trace of the orthogonalized $U_{ij}$ tensor.

**Table 4**
Comparison of selected bond distances in $Eu_{11}Cd_6Sb_{12}$ and $Eu_{11}Zn_6Sb_{12}$

| Atom pair ($M$ = Cd or Zn) | Distances (Å) | |
|---|---|---|
| | $Eu_{11}Cd_6Sb_{12}$ | $Eu_{11}Zn_6Sb_{12}$ |
| *M*1–Sb2 | 3.0716(8) | 3.015(2) |
| *M*1–Sb3 × 2 | 2.8805(5) | 2.762(1) |
| *M*1–Sb6 | 2.8512(8) | 2.723(2) |
| *M*2–Sb2 × 2 | 2.8133(4) | 2.701(1) |
| *M*2–Sb4 | 2.8672(8) | 2.737(2) |
| *M*2–Sb4 | 2.9876(8) | 2.893(2) |
| *M*3–Sb1 × 2 | 2.7710(4) | 2.6580(9) |
| *M*3–Sb4 | 2.9390(8) | 2.824(2) |
| *M*3–Sb5 | 3.1965(8) | 3.249(2) |
| Sb5–Sb5 | 2.812(1) | 2.795(2) |

### 2.4. Resistivity measurements

Measurements of the electrical resistivity as a function of the temperature were carried out using the four-probe method. For this purpose, a high accuracy *ac*-resistance bridge and a custom-built cryostat utilizing a closed-cycle He-refrigerator were employed. Data were collected within the temperature range 15–290 K on a single crystal of $Eu_{11}Cd_6Sb_{12}$ with dimensions of $1 \times 0.3 \times 0.2\ mm^3$. Four platinum wires (0.001″) were connected to the crystal using EPO TEK H20 silver epoxy; both heat-up and cool-down measurements were carried out on the same specimen to ensure reproducibility and in order to subtract any thermo-electric voltages formed at the junctions of dissimilar materials.

## 3. Results and discussion

### 3.1. Crystal structure

$Eu_{11}Cd_6Sb_{12}$ and $Eu_{11}Zn_6Sb_{12}$ are rare-earth metal analogs of $Sr_{11}Cd_6Sb_{12}$ and $Ba_{11}Cd_6Sb_{12}$ [22,23]. Their structures are best viewed as being made of isolated cations and a covalently bonded polyanionic sub-network of $CdSb_4$ or $ZnSb_4$ tetrahedra. They share common corners to form ribbons, which run parallel to the crystallographic *b*-direction (Fig. 1). The cations, i.e., $Sr^{2+}$, $Ba^{2+}$ and $Eu^{2+}$ provide the electrons needed for the bonding and fill the space within the polyanionic sub-lattice. An important characteristic of the structure is the presence of strong Sb–Sb interactions, which give rise to what was first described by Park and Kim [23] for $Sr_{11}Cd_6Sb_{12}$ as "an anisotropic infinite one-dimensional (1D) structure composed of double pentagonal tubes". This description bears resemblance with the structures of $Eu_{10}Mn_6Sb_{13}$ [16] and $Eu_{10}Cd_6Bi_{12}$ [20], which are also reported to have "double pentagonal channels"—note how close these compositions are to $Eu_{11}Cd_6Sb_{12}$. The structural relationships have been discussed in earlier publications [22,23]; however, there are several other ways to relate the structures of the title compounds to some simple and well-known structure types. One such parallel will be at the focus of our attention next.

Fig. 2 shows a schematic representation of how the structure of $Eu_{11}Cd_6Sb_{12}$ can be built of "modular" building blocks according to the equation:

$$2Eu_3CdSb_3 + Eu_5Cd_2Sb_6 + 2Cd \rightarrow Eu_{11}Cd_6Sb_{12}$$

The same approach can be used for the Zn analogs as well. This idea is extrapolated from an earlier report on the structures and bonding of $Ca_2CdSb_2$ and $Yb_2CdSb_2$ [19]. As already discussed therein, the bonding arrangements in the latter compounds can be derived from the structures of the equiatomic CaCdSb and YbCdSb with the TiNiSi structure type [29]. This "process" requires the removal of 1/2 of the Cd atoms from the equiatomic structure and an appropriate re-sizing of the unit cell in order to account for the new packing of the two-dimensional (2D) layers (in the resultant $Ca_2CdSb_2$ and $Yb_2CdSb_2$ structures). It can be further speculated that a subsequent removal of more cadmium could result in $A_3CdSb_3$, where the $^2_\infty[CdSb_2]$ layers will be broken into $^1_\infty[CdSb_3]$ chains (Fig. 2). Such compounds with 1D chains of corner-sharing $CdSb_4$ tetrahedra, as discussed elsewhere [22], are electron-deficient and are not likely to form; however, the very same bonding arrangement will have an optimal valence electron concentration if a group 13 element is at the center of the tetrahedra. This idea is nicely illustrated for example in the $^1_\infty[AlAs_3]$, $^1_\infty[AlSb_3]$ and $^1_\infty[InP_3]$ chains in the Zintl phases $Ca_3AlAs_3$ [36], $Ca_3AlSb_3$ [37] and $Eu_3InP_3$ [38], respectively. We also note here that if the hypothetical $^1_\infty[CdSb_3]$ chains, which are parallel to each other, are rearranged so that two of their vertexes come close together to form *exo*-bonds, a new structure with dimerized $^1_\infty[Cd_2Sb_6]$ chains will be obtained (Fig. 2). Due to the homoatomic Sb–Sb bonds, this structure will require two fewer electrons, i.e., the formulas of these imaginary phases will be $A_5Cd_2Sb_6$, not $A_6Cd_2Sb_6$ ($A$ = divalent cations). This point, again, is nicely evidenced in the Zintl phases $Ca_5Al_2Sb_6$ [39] and $Ca_5Ga_2As_6$ [40], for example, the structures of which feature double chains

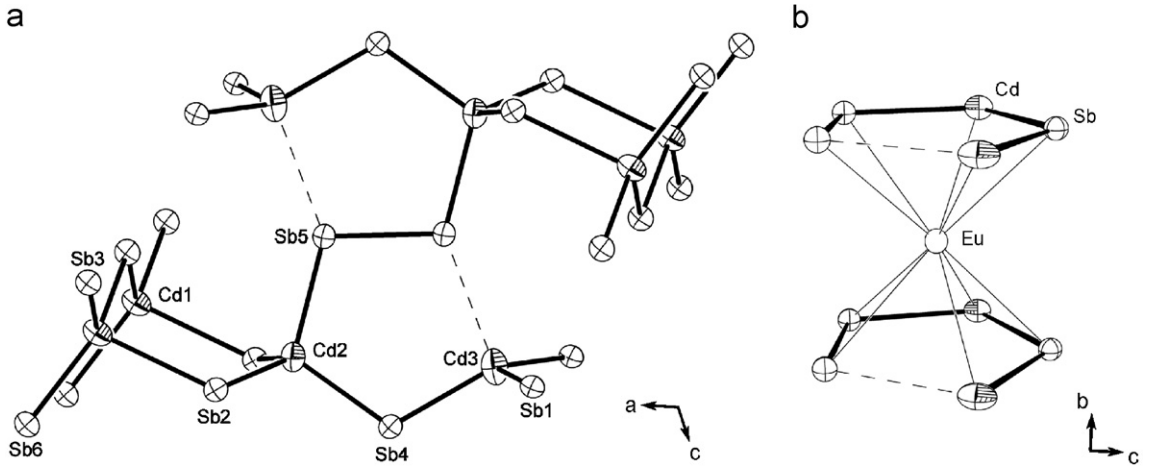


**Fig. 1.** (a) Perspective view of a segment of the monoclinic structure of $Eu_{11}Cd_6Sb_{12}$ and $Eu_{11}Zn_6Sb_{12}$ (Pearson's symbol *mC*58), viewed approximately down the *b*-axis. Anisotropic displacement parameters are drawn at the 95% probability level: Cd atoms are shown with full ellipsoids, Sb atoms are represented with crossed ellipsoids. The Eu atoms are not shown so that the connectivity mode of the $CdSb_4$ tetrahedra can be better illustrated. (b) Close view of the coordination polyhedron of Eu1. Relevant distances are given in Table 3.

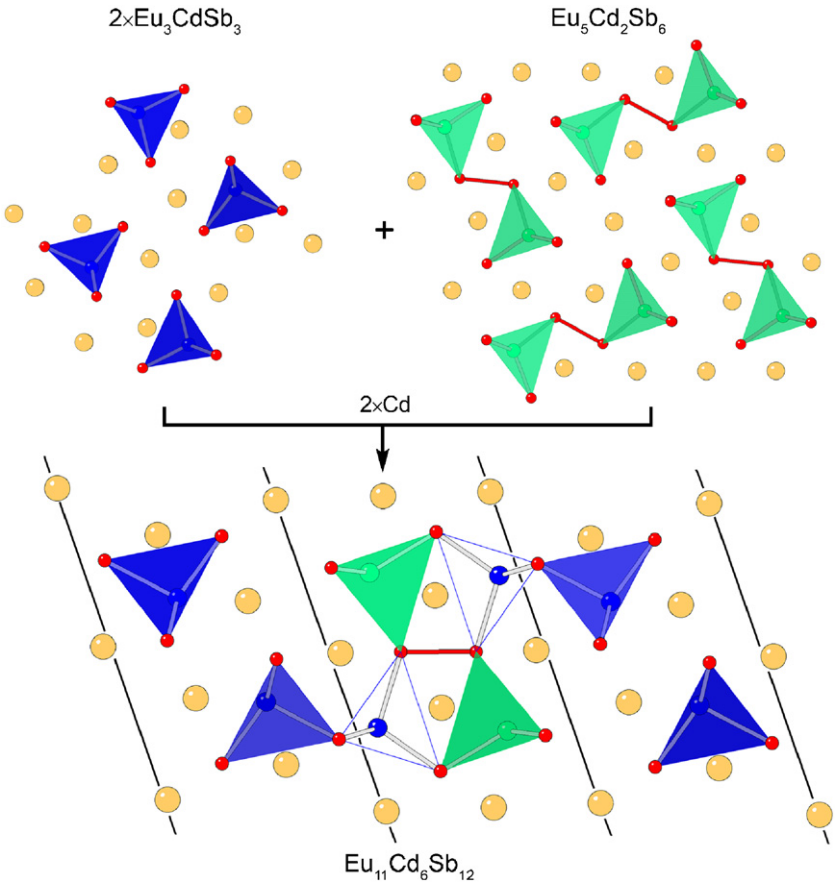


**Fig. 2.** Schematic representation of how the $Eu_{11}Cd_6Sb_{12}$ structure can be built from imaginary fragments of $Eu_3CdSb_3$ ($Ca_3AlAs_3$ structure type) and $Eu_5Cd_2Sb_6$ ($Ca_5Ga_2As_6$ structure type) and the addition of two extra cadmium atoms in the available tetrahedral holes. See text for further discussion.

with the above-described topology, $^1_\infty[Al_2Sb_6]$ and $^1_\infty[Ga_2As_6]$, respectively.

Having discussed these relationships, it is now easy to elucidate how the polyanionic $^1_\infty[Cd_6Sb_{12}]$ sub-network in $Eu_{11}Cd_6Sb_{12}$ can be viewed as an intergrowth of: (1) two corner-sharing chains, $^1_\infty[CdSb_3]$, which are topologically similar to the ones in the above-discussed compound $Eu_3CdSb_3$; and (2) a double chain, $^1_\infty[Cd_2Sb_6]$, bridged through a $Sb_2$ dimer, which is very much alike the chains in the aforementioned compound $Eu_5Cd_2Sb_6$. To complete the assembly, two additional cadmium atoms must be filled into the tetrahedral holes formed by these segments. This fully accounts for the structure and the stoichiometry of the ensuing compound $Eu_{11}Cd_6Sb_{12}$. Closer inspection of the $^1_\infty[Cd_6Sb_{12}]$ segment (Fig. 2) reveals that there are two more

tetrahedral sites, which if occupied by two extra cadmium atoms would ultimately result in 2D layers, $^{2}_{\infty}[Cd_8Sb_{12}]$. Such a double-layered structure is perhaps too crowded and definitely electron-rich, which can explain why nature in this case necessitates nearly 1/4 of the Cd sites to be vacant, leading to the electron-precise compound $Eu_{10}Cd_6Bi_{12}$ [20] instead.

Another important aspect of the structure under consideration, which warrants further discussion, is the unusually long contact between Cd3 and Sb5 and between Zn3 and Sb5. Table 4 lists a side-by-side comparison of some relevant distances. We draw the attention to the fact that the Zn3–Sb5 distance in $Eu_{11}Zn_6Sb_{12}$ is 3.249(2) Å, longer than the corresponding Cd3–Sb5 distance in $Eu_{11}Cd_6Sb_{12}$, 3.1965(8) Å. This is unexpected because Zn is smaller than Cd and the trend should have been reversed. Such line of thinking is supported by comparison of the all other Zn–Sb and Cd–Sb distances (Table 4). However, the trend seen when the Sb–Sb bond distances are compared across the series is very different. Surprisingly, they are almost invariant of the size of the cation—2.811(2) Å for $d_{Sb-Sb}$ in $Sr_{11}Cd_6Sb_{12}$ [22], 2.813(2) Å for $d_{Sb-Sb}$ in $Ba_{11}Cd_6Sb_{12}$ [22], and 2.812(1) Å in $Eu_{11}Cd_6Sb_{12}$. There is a small, albeit noticeable difference between the Sb–Sb distances in the Cd and Zn compounds, 2.812(1) Å in $Eu_{11}Cd_6Sb_{12}$ and 2.795(2) Å in $Eu_{11}Zn_6Sb_{12}$, respectively (recall that the aforementioned Cd3–Sb5 and Zn3–Sb5 contacts vary in opposite way).

This comparative analysis, together with the fact that the Cd3–Sb5 and Zn3–Sb5 distance are more than 20% longer than the sum of the corresponding Pauling's covalent radii [41] suggests that the latter represent very weak interactions and should not be considered as typical 2-center-2-electron bonds. These speculations are corroborated by a previous computational study using the tight-binding linear-muffin-tin-orbital (TB-LMTO-ASA) method [22], the results of which reveal the subtleties of this complex structure. Despite the possible difficulties assigning formal charges following the empirical rules for electron counting, the calculations suggest that the bonding is optimized, i.e., the polyanionic framework retains its Zintl-like electron requirements. In this sense, the structure can be rationalized as $[A^{2+}]_{11}[Cd_6Sb_{12}]^{22-}$ ($A$ = Sr, Ba, Eu).

### 3.2. Phase space

$Eu_{11}Cd_6Sb_{12}$ and $Eu_{11}Zn_6Sb_{12}$ are new compounds in the respective ternary systems, where only the following three phases are already known: $Eu_9Cd_4Sb_9$ [26], $EuCd_2Sb_2$ [42] and $EuZn_2Sb_2$ [43]. Attempts to synthesize the Sr analog of $Eu_{11}Zn_6Sb_{12}$ were unsuccessful (see Experimental), which is seemingly at odds with the fact that the pair $Eu_{11}Cd_6Sb_{12}/Sr_{11}Cd_6Sb_{12}$ does exist and that the ionic radii of $Sr^{2+}$ and $Eu^{2+}$ are very close [44]. While unexpected, such a peculiarity can be related to other precedents among Sr- and Eu-intermetallics that have "missing" (or structurally unrelated) counterparts. Take for example $EuGe_2$ [45,46], which crystallizes with the trigonal space group $P\bar{3}m1$ (no. 164) and $SrGe_2$, which is known to be dimorphic [29]—the ambient conditions polymorph is orthorhombic (*Pnma*, no. 62) [47], while the form that is isostructural with $EuGe_2$ is actually stabilized at high pressures [48]. As a different example can be pointed $EuBi_2$ [49] with an orthorhombic structure that is related to the $ZrSi_2$ type—it does not appear to have a known Sr analog [29,50].

Another possible explanation for the "missing" $Sr_{11}Zn_6Sb_{12}$ can be brought if one recalls earlier reports, which indicate a very delicate balance between the packing (atomic sizes) and electronic requirements (valence electron count) in the related structures of the $Ca_2CdSb_2$ [19] and $Sr_9Cd_{4.49(1)}Sb_9$ [26]. These studies suggest that the size difference between the $Ca^{2+}$ cations in $Ca_2CdSb_2$ and the $Sr^{2+}$ cations in $Sr_9Cd_{4.49(1)}Sb_9$ is responsible for the preference of one structure type over the other (note that the stoichiometry is virtually identical). Another relevant example is the pair $Ca_2CdSb_2/Yb_2CdSb_2$ [19], which have the same composition, electronic requirements and similar sizes for the cations, but have subtly different structures. DFT calculations for those arrangements suggest that despite the resemblance, the structures show distinct cation preferences [19], which could also be the case here. A proof that this explanation is also applicable to the $Eu_{11}Cd_6Sb_{12}$ structures is the formation of the mixed-cation phase $Eu_{11-x}Ca_xCd_6Sb_{12}$ [51]. This structure was refined from single-crystal X-ray diffraction data to have mixed occupancy of Ca and Eu on all sites, except the one, which is centering the pentagonal tubes, Eu1 in the current notation. Apparently this cationic position is not suitable for the smaller $Ca^{2+}$ cations [44] due to its special coordination (similar to Fe in the eclipsed configuration of ferrocene, Fig. 1b), and therefore, stoichiometric $Ca_{11}Cd_6Sb_{12}$ is not likely to exist.

Similar arguments can be used to address our inability to synthesize any bismuthides that are isostructural or closely related to $Eu_{11}Zn_6Sb_{12}$ or $A_{11}Cd_6Sb_{12}$ ($A$ = Sr, Ba, Eu). One could argue that apparent difficulty is due to the lower melting point of Bi compared to that of Sb, the optimal synthetic conditions are not established yet. However, we feel that it might also be explained by the difference in sizes between bismuth and antimony—the larger bismuth anions cannot pack efficiently with small cations such as $Sr^{2+}$ or $Eu^{2+}$. One could also argue that if this is the case, the best chances of synthesizing a bismuthide with this structure will be with $Ba_{11}Cd_6Bi_{12}$; however, repeated attempts proved fruitless. A logical assumption for this "failure" is that the Cd–Bi interactions in $Ba_{11}Cd_6Bi_{12}$ are not as strong as in some other ternary phases such as $Ba_{11}Cd_8Bi_{14}$ [18], $Ba_{21}Cd_4Bi_{18}$ [21], or $Ba_2Cd_3Bi_4$ [25]. Since these compounds were the typical products of all Ba–Cd–Bi reactions that were carried out (see Experimental), we may speculate that $Ba_{11}Cd_6Bi_{12}$ is thermodynamically unstable with respect to those compounds and/or some of the known binary Ba–Cd or Ba–Bi phases [29]. Ba–Zn–Bi reactions aimed at $Ba_{11}Zn_6Bi_{12}$ were tried, but were also unsuccessful.

### 3.3. Magnetic susceptibility

Fig. 3 shows plots of the magnetic susceptibility ($\chi_m$) and the inverse susceptibility ($1/\chi_m$) as a function of the temperature ($T$) for both compounds. A cusp-like feature is visible in the $\chi_m(T)$ data at $T_N = 7.5$ K for $Eu_{11}Cd_6Sb_{12}$ as determined from the mid-point in the jump in $d\chi/dT$, respectively. This indicates the onset of a long-range antiferromagnetic (AFM) order. No peak is seen in the $\chi_m(T)$ data for $Eu_{11}Zn_6Sb_{12}$, although it is possible that it may also undergo AFM transition below 5 K, the lowest attained temperature.

Above ca. 10 K (above $T_N$), the inverse susceptibility, in both cases, increases linearly with the temperature indicating, that it follows the Curie–Weiss law [52]. From the Curie constant, the effective paramagnetic moments were calculated to be $\mu_{eff} = 7.80$ and 7.68 $\mu_B$ for $Eu_{11}Cd_6Sb_{12}$ and $Eu_{11}Zn_6Sb_{12}$, respectively. Both values are in agreement with the effective paramagnetic moment for free $Eu^{2+}$ ions according to $\mu_{eff} = g[J(J+1)]^{1/2} = 7.94\,\mu_B$ [52]. The Weiss temperatures are negative for both compounds: $\Theta_{CW} = -2.1$ for $Eu_{11}Cd_6Sb_{12}$ and $\Theta_{CW} = -1.5$ K for $Eu_{11}Zn_6Sb_{12}$, as expected for AFM-ordered phases.

### 3.4. Electrical resistivity

Fig. 4 shows the electrical resistivity of $Eu_{11}Cd_6Sb_{12}$. Inspecting its temperature dependence reveals the weakly metallic behavior of the compound—the resistivity rises with the temperature

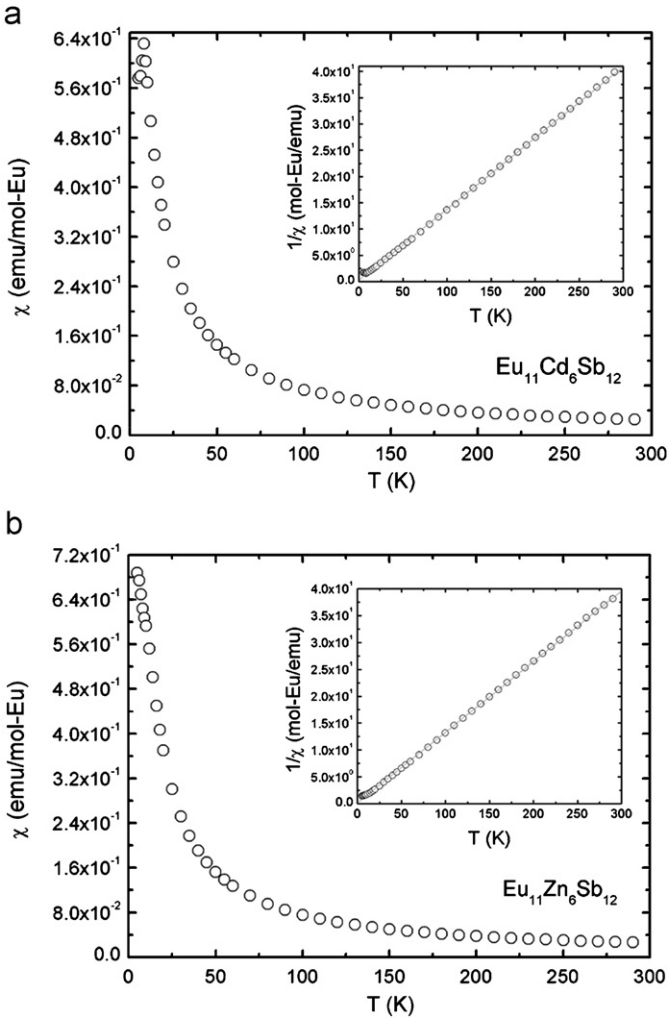


**Fig. 3.** Magnetic susceptibility ($\chi_m = M/H$) vs. temperature ($T$) of (a) $Eu_{11}Cd_6Sb_{12}$ and (b) $Eu_{11}Zn_6Sb_{12}$. The insets show the fit of the inverse susceptibility to the Curie–Weiss law $\chi_m = C/(T-\Theta_{CW})$. The measurements (5–290 K) are done on polycrystalline samples using an applied magnetic field $H = 500$ Oe.

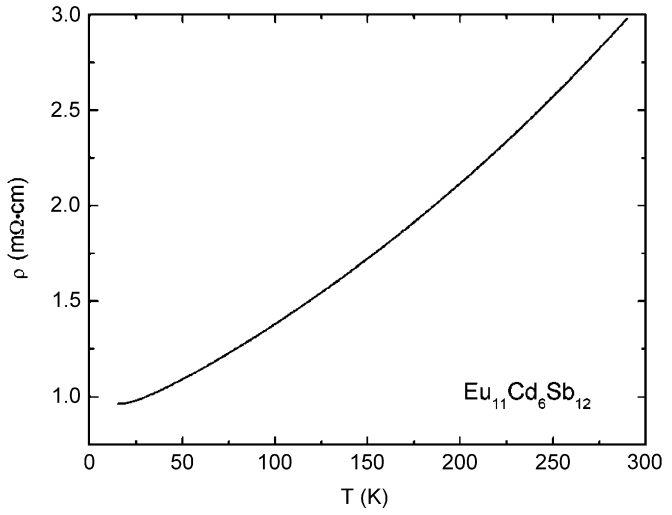


**Fig. 4.** Resistivity ($\rho$) as a function of temperature ($T$) measured on single-crystal of $Eu_{11}Cd_6Sb_{12}$.

reaching a room temperature value of approximately $\rho_{290} = 3$ mΩ cm. This, together with the slope of the curve is indicative of a poorly metallic conductance, in agreement with the DOS calculations for this structure reported previously [22], and the Zintl-like electron count discussed above. The calculations also predict an anisotropic electrical conductivity; however, due to the small crystal size, this theoretical result could not be confirmed experimentally—reliable measurement was obtained only in a direction of the needle, presumed to be the shortest crystallographic direction, the *b*-axis (Table 1).

Since large single crystals of $Eu_{11}Zn_6Sb_{12}$ could not be obtained, a polycrystalline pellet was prepared under hydrostatic pressure at room temperature. It was measured but its resistance was very low—two orders of magnitude lower than that of $Eu_{11}Cd_6Sb_{12}$, suggesting that residual Pb flux or an impurity phase hampered the measurement. As there is no indication to suggest any differences in the physical properties of these isostructural compounds, we speculate that $Eu_{11}Zn_6Sb_{12}$ is expected to have similar resistivity to $Eu_{11}Cd_6Sb_{12}$.

## 4. Conclusions

The synthesis, crystal structure from single-crystal X-ray diffraction and magnetic properties of $Eu_{11}M_6Sb_{12}$, where $M$ = Cd, Zn have been reported. Both compounds crystallize with the monoclinic $Sr_{11}Cd_6Sb_{12}$-type structure, which is built of $MSb_4$ tetrahedra. Detailed structural relationships, including analysis of various bonds, comparisons, coordination environments and derivation from simple and well-known structure types, are provided. The magnetic susceptibility of both compounds suggests that Eu cations are divalent in both $Eu_{11}Cd_6Sb_{12}$ and $Eu_{11}Zn_6Sb_{12}$. Temperature-dependent resistivity measurement indicates poor metallic behavior of $Eu_{11}Cd_6Sb_{12}$. The rich crystal chemistry of this structure and the modular approach we describe in order to explain it might be a good starting point for the exploration new ternary phases of the alkaline-earth and divalent rare-earth metals, the $d^{10}$ metals and the pnicogens.

## Acknowledgments

Svilen Bobev acknowledges the University of Delaware (start-up grant) and the Donors of the American Chemical Society Petroleum Research Fund for the financial support of this research.

## References

[1] H. Schäfer, B. Eisenmann, W. Müller, Angew. Chem. Int. Ed. Engl. 12 (1973) 694.
[2] J.D. Corbett, Angew. Chem. Int. Ed. 39 (2000) 670.
[3] S.M. Kauzlarich (Ed.), Chemistry, Structure, and Bonding of Zintl Phases and Ions, VCH Publishers, Inc., New York, 1996.
[4] J.Y. Chan, M.M. Olmstead, S.M. Kauzlarich, Chem. Mater. 10 (1998) 3583.
[5] J.Y. Chan, S.M. Kauzlarich, P. Klavins, R.N. Shelton, D.J. Webb, Phys. Rev. B 57 (1998) R8103.
[6] I.R. Fisher, T.A. Wiener, S.L. Bud'ko, P.C. Canfield, J.Y. Chan, M.M. Olmstead, S.M. Kauzlarich, Phys. Rev. B 59 (1999) 13829.
[7] S.R. Brown, S.M. Kauzlarich, F. Gascoin, G.J. Snyder, Chem. Mater. 18 (2006) 1873.
[8] F. Gascoin, S. Ottensmann, D. Stark, S.M. Haile, G.J. Snyder, Adv. Funct. Mater. 15 (2005) 1860.
[9] S.M. Kauzlarich, S.R. Brown, G.J. Snyder, Dalton Trans 21 (2007) 2099.
[10] F. Gascoin, S.C. Sevov, Inorg. Chem. 41 (2002) 5920.
[11] F. Gascoin, S.C. Sevov, Inorg. Chem. 42 (2003) 904.
[12] H. Kim, C.L. Condron, A.P. Holm, S.M. Kauzlarich, J. Am. Chem. Soc. 122 (2000) 10720.
[13] A.C. Payne, A.E. Sprauve, M.M. Olmstead, A. Kauzlarich, J.Y. Chan, B.A. Reisner, J.W. Lynn, J. Solid State Chem. 163 (2002) 498.
[14] S.M. Park, S.J. Kim, M.G. Kanatzidis, Inorg. Chem. 44 (2005) 4979.
[15] S. Bobev, J. Merz, A. Lima, V. Fritsch, J.D. Thompson, J.L. Sarrao, M. Gillessen, R. Dronkowski, Inorg. Chem. 45 (2006) 4047.

[16] A.P. Holm, S.M. Park, C.L. Condron, M.M. Olmstead, H. Kim, P. Klavins, F. Grandjean, R.P. Herman, G.J. Long, M.G. Kanatzidis, S.M. Kauzlarich, S.J. Kim, Inorg. Chem. 42 (2003) 4660.
[17] S.Q. Xia, S. Bobev, Inorg. Chem. 46 (2007) 874.
[18] S.Q. Xia, S. Bobev, Inorg. Chem. 45 (2006) 7126.
[19] S.Q. Xia, S. Bobev, J. Am. Chem. Soc. 129 (2007) 4049.
[20] S.Q. Xia, S. Bobev, Chem. Asian J. 2 (2007) 619.
[21] S.Q. Xia, S. Bobev, Inorg. Chem. 47 (2008) 1919.
[22] S.Q. Xia, S. Bobev, J. Comp. Chem. (2008) doi:10.1002/jcc.20983.
[23] S.M. Park, S.J. Kim, J. Solid State Chem. 177 (2004) 3418.
[24] P.C. Canfield, Z. Fisk, Philos. Mag. B 65 (1992) 1117.
[25] S.Q. Xia, S. Bobev, J. Solid State Chem. 179 (2006) 3371.
[26] S.Q. Xia, S. Bobev, J. Am. Chem. Soc. 129 (2007) 10011.
[27] A. Mewis, Z. Naturforsch. 33B (1978) 382.
[28] D.M. Young, C.C. Torardi, M.M. Olmstead, S.M. Kauzlarich, Chem. Mater. 7 (1995) 93.
[29] P. Villars, L.D. Calvert (Eds.), Pearson's Handbook of Crystallographic Data for Intermetallic Compounds, second ed, American Society for Metals, Materials Park, OH, 1991 and the desktop edition, 1997.
[30] The crystals of $Sr_{21}Cd_4Sb_{18}$ (Sb-analog of the known $Sr_{21}Cd_4Bi_{18}$ [Ref. 21]) were obtained as a byproduct of a reaction of Sr, Cd, and Sb in a ratio 1:1:1:2 (Pb flux). Space group $C2/m$. Unit cell dimensions: $a = 18.2460(15)$ Å, $b = 17.3949(15)$ Å, $c = 17.3673(15)$ Å, $\beta = 92.026(1)^\circ$, $V = 5674(1)$ Å$^3$. CSD 419362.
[31] JADE Version 6.5, Materials Data, Inc., Livermore, CA, 2003.
[32] SMART NT Version 5.6, Bruker Analytical X-ray Systems, Inc., Madison, WI, 2003.
[33] SAINT NT Version 6.4, Bruker Analytical X-ray Systems, Inc., Madison, WI, 2003.
[34] SADABS NT Version 2.1, Bruker Analytical X-ray Systems, Inc., Madison, WI, 2001.
[35] SHELXTL Version 6.1, Bruker Analytical X-ray Systems, Inc., Madison, WI, 2001.
[36] G. Cordier, H. Schäfer, Angew. Chem. Int. Ed. Engl. 20 (1981) 466.
[37] G. Cordier, H. Schäfer, M. Stelter, Z. Naturforsch. 39B (1984) 727.
[38] J. Jiang, A.C. Payne, M.M. Olmstead, H. Lee, P. Klavins, Z. Fisk, S.M. Kauzlarich, R.P. Hermann, F. Grandjean, G.J. Long, Inorg. Chem. 44 (2005) 2189.
[39] G. Cordier, E. Czech, M. Jakowski, H. Schäfer, Rev. Chim. Miner. 18 (1981) 9.
[40] P. Verdier, P. L'Haridon, M. Maunaye, Y. Laurent, Acta Crystallogr. B 32 (1976) 726.
[41] L. Pauling, The Nature of the Chemical Bond, third ed, Cornell University Press, Ithaca, NY, 1960.
[42] A. Artmann, A. Mewis, M. Roepke, G. Michels, Z. Anorg. Allg. Chem. 622 (1996) 679.
[43] F. Weber, A. Cosceev, A. Nateprov, C. Pfleiderer, A. Faist, M. Uhlarz, H.V. Löhneysen, Physica B 359–361 (2005) 226.
[44] R.D. Shannon, Acta Crystallogr. A 32 (1976) 751.
[45] S. Bobev, E.D. Bayer, J.D. Thompson, J.L. Sarrao, G.J. Miller, B. Eck, R. Dronskowski, J. Solid State Chem. 177 (2004) 3545.
[46] E.I. Gladyshevskii, Dokl. Akad. Nauk Ukr. RSR 2 (1964) 209.
[47] A. Betz, H. Schäfer, A. Weiss, R. Wulf, Z. Naturforsch. B 23 (1968) 878.
[48] J. Evers, G. Oehlinger, A. Weiss, Z. Naturforsch. B 34 (1979) 524.
[49] Z. Sun, J. Mao, J. Solid State Chem. 177 (2004) 3752.
[50] T.B. Massalski (Ed.), Binary Alloy Phase Diagrams, second ed, American Society for Metals: Materials Park, OH, 1990.
[51] The crystals of $Eu_{9.8}(2)Ca_{1.2}(2)Cd_6Sb_{12}$ were obtained as a byproduct of a reaction of Ca, Eu, Cd, and Sb in a ratio 1:1:1:2 (Pb flux). Temperature profile was the same as for $Eu_{11}Cd_6Sb_{12}$. The main product of the reaction was $Ca_2CdSb_2$ [Ref. 19]. Unit cell dimensions: $a = 32.383(3)$ Å, $b = 4.7256(4)$ Å, $c = 12.3673(11)$ Å, $\beta = 109.956(1)^\circ$, $V = 1778.9(3)$ Å$^3$. CSD 419342.
[52] C. Kittel, Introduction to Solid State Physics, seventh ed, Wiley, Hoboken, NJ, 1996.